Fatigue sensitivity to foundation modelling in different operational states for the DTU 10MW monopile-based offshore wind turbine

IOP Conf. Series: Journal of Physics: Conf. Series **1356** (2019) 012019 doi:10.1088/1742-6596/1356/1/012019

Fatigue sensitivity to foundation modelling in different operational states for the DTU 10MW monopile-based offshore wind turbine

George Katsikogiannis[1*], Erin E. Bachynski[1], Ana M. Page[2]

[1]Department of Marine Technology, Norwegian University of Science and Technology, N7491 Trondheim, Norway
[2]Norwegian Geotechnical Institute, Sognsvn. 72, N-0855 Oslo, Norway

*Email: george.katsikogiannis@ntnu.no

Abstract. The importance of foundation modelling for the support-structure fatigue damage estimation of a 10 MW monopile based offshore wind turbine is investigated in different operational states and wind-wave misalignment conditions. Three different models are used: (1) a non-linear elasto-plastic model including hysteretic behaviour effects, (2) a linear elastic model and (3) a non-linear elastic model, using numerical simulations with an aero-hydro-servo-elastic computational tool. Depending on the environmental condition, different dynamic processes dominate the responses. For parked states, deviations between models up to 160% were found. For wind wave-misalignment over 30° in operational cases, differences up to 180% were found for low sea states and 119% for high sea sates. Both nonlinear foundation damping and stiffness formulation have considerable effect on the responses, with hysteretic effects becoming crucial when aerodynamic damping is negligible in the direction of the response. Attention is required when comparing the fatigue damage only at the mudline, as larger variations between the models may occur in the embedded part of the monopile, where the absolute maximum is found.

1. Introduction

The offshore wind industry is growing fast, becoming a mainstream supplier of low-carbon electricity and it is expected to produce 7% to 11% of the EU's electricity demand by 2030 [1]. Offshore wind farm developments are also growing in size, with their average capacity reaching 493 MW in 2017 [2].

The main challenge for future offshore wind farm developments is to reduce the levelized cost of energy (LCOE). The LCOE has lately been reduced by the use of larger capacity turbines and improved supply chain integration [3], however further cost reduction can be achieved by more efficient designs of offshore wind turbines (OWTs). The OWT foundation, defined as the part of the support structure which transfers the loads acting on the structure into the seabed [4], has a high potential for cost reduction, as it contributes up to 20% of total capital costs [5].

Monopiles represent approximately 82% of all installed substructures in Europe [2]. It is anticipated that monopiles will remain a preferred choice due to manufacturing speed and fabrication experience [6]. With the gradual introduction of higher capacity OWTs (6–10 MW) for deeper water wind farms, large-diameter monopiles are considered to be one of the most promising options, testing however various technical and economical limits.

Monopile-based OWTs design, relies on dynamic analyses, coupling aerodynamics, hydrodynamics, soil-structure interaction (SSI) and control system aspects. Due to the pronounced dynamic responses,

fatigue is one of the governing factors for the final design. Fatigue damage assessment is a time-consuming, complex process, and the results are sensitive to variations in the OWT operational state, loading environment and foundation modelling. Several studies have demonstrated the effect of the foundation on natural frequency and structural fatigue damage of OWTs [7-10]. Although considerable development has been made on representing the interaction between wind, waves and structural response aspects in OWT dynamic analyses, the foundation modeling remains unrefined in most existing models [11]. The current industry design practice in foundation modelling for monopiles is based on *p-y* curves. In the *p-y* curves approach, the soil response is idealized by means of uncoupled, non-linear springs, which support the monopile along the embedded length. In particular, discrepancies between API *p-y* curves [12] and large-diameter monopile behavior have been identified [13], and their adequacy to represent accurately the monopile behavior has been questioned.

In order to address some of these discrepancies, a new foundation model for monopiles based on macro-element approach has been proposed [14]. The macro-element model incorporates some of the observed soil and foundation features that are not accounted for in the *p-y* curves formulation, such as different stiffness during loading-unloading, soil hysteretic effects, soil damping and coupling between multidirectional loads. Some first studies have indicated that the proposed model predicts lower fatigue damage compared to various SSI models, such as the *p-y* element approach or linear elastic stiffness matrix [8]. However, these studies do not take into account the coupling between loads in different directions, which is important for wind-wave misalignment conditions. For wind-wave misalignment or parked situations, aerodynamic damping may not be effective in the load direction, and the details of foundation modelling become relatively more important for the structural response.

The aim of the present study is to investigate the effect of including hysteretic foundation behavior through a macro-element model on the fatigue lifetime of a large diameter monopile foundation for different operational-environmental states. Comparisons are made between the macro-element model and different foundation models calibrated to provide an equivalent stiffness response.

2. Foundation Behaviour

The response of large-diameter monopiles is dominated by large horizontal loads, which combined with the height of the structure, result in large bending moments at mudline. The applied axial loads are relatively small compared to the horizontal forces [15]. In addition, large-diameter monopiles are characterized by a low length-to-diameter ratio (L/D). This results in a relatively rigid structural behavior, different from flexible bending beam behavior assumed in the API *p-y* curves formulation.

2.1. Main aspects of soil behaviour affecting monopile foundation response

The response of monopile foundations depends on the response of the surrounding soil. Specifically, the main aspects of soil behavior which affect monopile response are:

1. *Soil stiffness*. Soils exhibit a non-linear response that leads to different soil stiffness during loading, unloading and reloading. As a result, the monopile load-displacement response is non-linear and hysteretic. Variations in foundation stiffness can bring the OWT natural frequencies closer to the excitation. Realistic representation of the foundation stiffness under cyclic loading is essential for the accurate prediction of the foundation fatigue damage.

2. *Soil damping.* Soils dissipate energy by geometric spreading of waves (radiation damping) and by plastic deformation (hysteretic damping) [11]. The energy dissipated by radiation damping is negligible for frequencies below 1 Hz, thus negligible for monopile foundation analysis [16]. Hysteretic damping becomes the main soil damping contributor. The individual contributions from aerodynamic, hydrodynamic, structural and soil damping vary for different situations [16-19]. Aerodynamic damping provides the highest contribution to the overall damping, however its importance decreases in parked and wind-wave misalignment situations, resulting in increased relative importance of soil damping.

2.2. Foundation modelling in offshore wind turbine design

Dynamic simulations are usually used to determine OWT load effects for OWT design [4]. Generally, industry makes use of approaches where the support structure and wind turbine are simulated separately, using super-imposed or semi-integrated load calculation approaches [18]. However, a fully-integrated analysis is often required to capture the interaction between the various loads and structural response, making appropriate assumptions regarding soil stiffness and damping. In a fully-integrated analysis, the entire OWT - rotor-nacelle assembly, support structure, foundation - is subjected to simultaneous aerodynamic and hydrodynamic loads incorporating control system and SSI aspects.

The most common approach used for modelling the monopile foundation response is the *p-y* curve approach, where *p* represents the soil lateral resistance and *y* the pile displacement. Often, *p-y* curves have been calibrated following the API *p-y* formulation. However, employing the API *p-y* formulation in the estimation of OWT dynamic response results in discrepancies between simulated and measured responses [17]. This is because [13] the API formulation was initially developed and validated for long, slender piles. Monopiles are less slender and show a more rigid behavior, such that neglecting other components of soil resistance, such as side and base shear, may lead to inaccurate prediction of the responses [20-23]. Additionally, the API *p-y* curves do not accurately reproduce the initial lateral foundation stiffness [7, 21] and as they are usually modelled as non-linear elastic, the contribution of hysteretic damping, due to plastic deformations, is not considered. Various formulation models have been proposed due to the API *p-y* curves limitations. A detailed review can be found in [11].

2.3. Macro-element foundation modelling

An alternative approach that can accurately and efficiently represent both the foundation stiffness and damping is macro-element modelling. These models condense the foundation and surrounding soil response to a force-displacement relation at one point, commonly located at mudline [21]. The response at this point is estimated from numerical analyses of the structure and soil (i.e. FEA) or experimentally. The macro-element modelling approach [14, 23] is able to include the contribution of soil resistance components such as base and side shear, which are not included in traditional *p-y* formulation. Moreover, depending on the model capability-complexity, it can account for various fundamental effects such as change of the overall stiffness due to non-linear hysteretic behaviour and hysteretic damping effects. Finally, the foundation response is only computed at one node, resulting in fewer degrees of freedom in the full structural model for integrated analysis than for the *p-y* approach.

The macro-element concept has been applied for jack-up spudcan foundations [20, 22], skirted foundations for OWTs [23], or foundations for bridges [24]. A new macro-element model based on the multi-surface plasticity formulation [25] has been developed [26] for predicting the load-displacement response and the hysteretic damping of monopile-based OWTs. Its formulation is based on results from FEA of the soil and the foundation. The performance of the macro-element model was compared against field test measurements and FEA results for three piled foundations and the model can reproduce the non-linear load-displacement response and the hysteretic behavior observed in monopiles with different L/D ratios [14]. Good agreement was also found between the model predictions and the FEA results while the macro element approach provides considerable reduction in computational effort.

3. Methodology

3.1. Wind Turbine Model

The wind turbine model is based on the DTU 10MW reference wind turbine (DTU 10MW RWT) [27], supported on a monopile foundation with a diameter of 9 m, thickness 0.11 m and penetration length of 36 m. It has a hub height of 119 m relative to the mean sea-water level and a rotor diameter of 178.3 m with a cut-in wind speed 4 m/s and cut-out speed 25 m/s. The wind inflow simulations were performed with TurbSim [28]. The wind turbine is modelled in SIMO-RIFLEX, an aero-hydro-servo-elastic finite-

element method simulation tool developed by SINTEF Ocean. Figure 1 shows the wind turbine model, including the support structure and the rotor-nacelle assembly (RNA). Three foundation models were used in the study and their detailed description can be found in section 3.3. Blade element momentum (BEM) theory is applied for aerodynamic load calculation. The hydrodynamic loads were based on a 1st order wave model with forces integrated up to the instantaneous undisturbed water line (assuming constant velocity potential above still water level). The MacCamy- and Fuchs formulation was used for environmental conditions (ECs) 1 - 4, to account for near-field diffraction effects, while Morison's equation was applied for EC5.

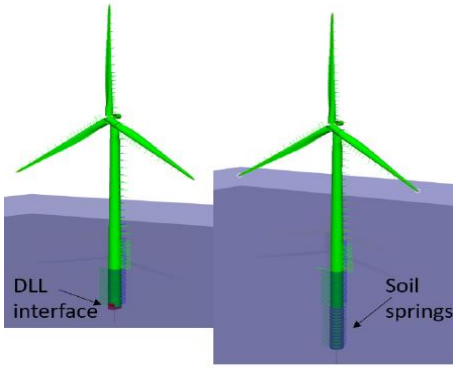

Figure 1 Wind Turbine model in SIMO-RIFLEX

3.2. Environmental Conditions

A numerical hindcast model from the National Kapodistrian University of Athens (NKUA) was used to generate 10-yr statistics for several locations in the North Sea, Atlantic Ocean and Mediterranean Sea for the Marina Platform project [29]. The hindcast data have resolution of 1 hour for the period 2001 to 2010 for a site located at the Norwegian Continental Shelf (NCS) with geographic coordinates 55.11°N, 3.47°E in 30 m water depth. The dataset provides information about metocean parameters such as mean wind speed (U_w), significant wave height (H_s), wave peak period (T_p) and wind-waves directionality. The turbulence conditions used in the study are based on the recommended practice [4]. A Kaimal wind spectrum with turbulence according to the normal turbulence model (NTM) for Class A turbines was used. Note that this represents very high turbulence intensity for offshore conditions. Wind shear is accounted for by the power law with exponent $\alpha = 0.14$ [4]. Table 1 shows a summary of the ECs analysed. In all simulations the OWT rotor is facing the wind, meaning that the wind direction coincides with the fore-aft (FA), therefore the wind-wave misalignment is the angle between the wave and the FA direction. For all the ECs, the OWT has been tested in both operational and parked states. In the latter case, the rotor is kept locked and the blades pitched to 90°. The sea-states used for the analyses were chosen as the ones that contribute the most to the long-term fatigue for five wind bins of 2 m/s, based on a long-term fatigue damage analysis for the given site considering unidirectional metocean data.

Table 1 Environmental conditions of the cases investigated

Simulation & Environmental Parameters						
EC number	Time Simulation [s]	U_w [m/s]	H_s [m]	T_p [s]	Wind-Wave Misalignment [degrees]	Wave Spectrum
1	3600	5.06	0.75	5.50	0, 15, 30, 45, 90	Pierson–Moskowitz
2	3600	9.06	1.25	5.50		Pierson–Moskowitz
3	3600	14.94	2.25	6.50		Torsethaugen
4	3600	20.90	3.75	7.50		JONSWAP
5	3600	26.74	5.25	8.50		JONSWAP

3.3. Foundation models

Three modelling approaches have been used to simulate the foundation response.

1. *Model 1 (M1). Macro-element model calibrated to FEA*. The elasto-plastic macro-element model with kinematic hardening [26] has been employed in this study. The model can represent the non-linear hysteretic load-displacement response observed in experimental tests and in the field [30] including coupled response between lateral loads and bending moment [14, 26]. A

general description of the model is given in section 2.3. The macro-element model is calibrated with load-displacement curves from Finite Element Analysis (FEA) of the soil (described by constitutive models) and the monopile foundation, as shown by Page et al. [26]. The model communicates with SIMO-RIFLEX through a dynamic link library (see Figure 1).

2. *Model 2 (M2). Linear elastic stiffness matrix with additional soil damping.* The stiffness matrix is applied at mudline and has been calibrated based on M1 to represent the monopile-foundation response at representative load levels. Soil damping is included in the form of stiffness-proportional Rayleigh structural damping applied to the sub-structure and tower. To quantify the contribution of foundation damping, a free vibration analysis with no wind and no waves was conducted for model M1. The analysis was performed by gradually applying a force of 1.5MN at the tower top and then releasing the force to allow the OWT to vibrate. Global damping was then quantified from the time history of the FA bending moment at the mudline using the logarithmic decrement method, where the logarithmic decrement (δ) is defined as:

$$\delta = \ln\left(\frac{A_i}{A_{i+1}}\right) = 2\pi\frac{\xi}{\sqrt{1-\xi^2}} \approx 2\pi\xi \qquad (1)$$

where A_i and A_{i+1} are two successive amplitudes and ξ is the global damping ratio. A comparison of the FA bending moment at the mudline from the free-vibration test and the global damping ratio for M1 and M2 with 0% and 0.6% soil damping is shown in Figure 2. The soil damping is chosen as 0.64% of the critical damping in order to have a reasonable approximation to the damping in M1. The value is similar to findings from different studies [31, 32] and within the range of theoretically calculated foundation damping [33]. Stiffness-proportional Rayleigh damping was tuned to capture the linear damping of the 1st natural frequency of the structure. (No mass-proportional term was included). The nonlinear damping in the M1 model can be seen in the nonzero slope of the damping ratio with respect to response amplitude (Figure 2, right).

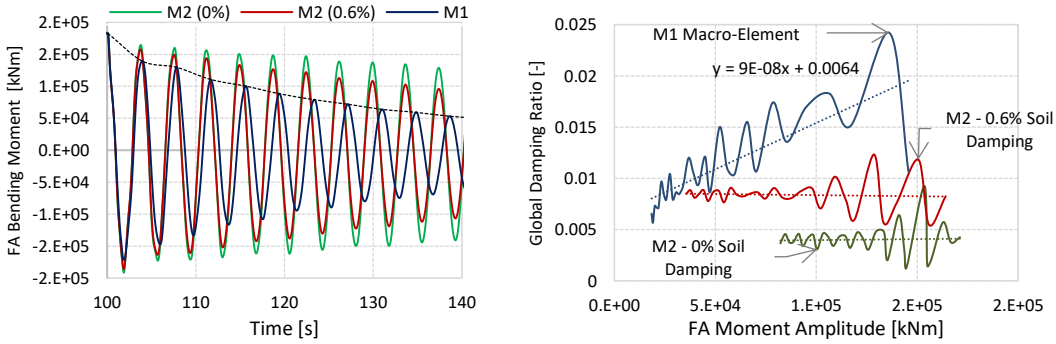

Figure 2 Decay test (left) and global damping ratio (right) for M1 and M2 with different levels of soil damping

3. *Model 3 (M3). P-Y curves calibrated to FEA*. The third model is a p-y curve model calibrated to same results of full 3D FEA [26] as described for M1. The monopile below the mudline is modelled as a beam and the soil is represented a series of discrete, uncoupled, elastic springs at nodal points along the pile. For M3 the same amount of soil damping as in M2 (0.64%) in the form of Rayleigh structural damping is added to the model. Figure 3 shows the static FA bending moment along the monopile when subjected to a constant force at the hub height.

Figure 4 presents the first fore-aft (FA) support structure natural frequencies from the different models, evaluated during the free decay tests. The natural frequencies of M1 and M3 depend on the moment amplitude, meaning that higher load levels result in lower foundation stiffness and consequently in lower natural frequencies. M2 is a linear elastic model, with constant eigenfrequency.

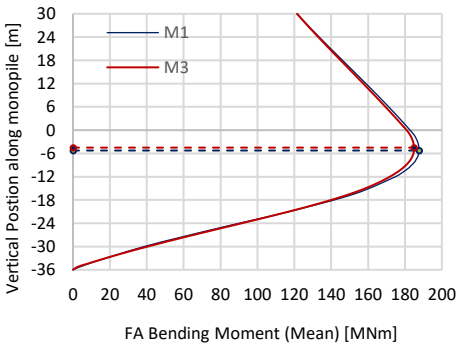

Figure 3 Static FA bending moment along monopile for M1-M3

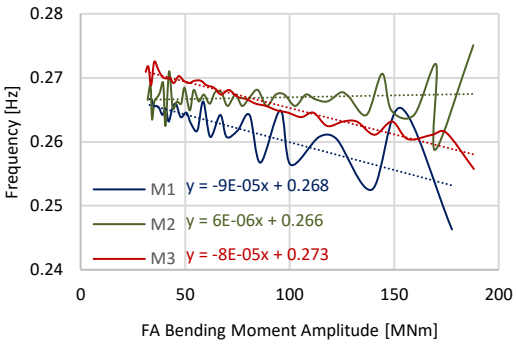

Figure 4 Eigenfrequencies for the foundation models

3.4. Stress and Fatigue Damage Calculation

The dynamic simulation results give the time history of loads at various cross sections along the monopile, denoted as N_x (axial force), M_y and M_z (bending moments). Based on the coordinate system in Figure 5, the axial stress (σ_x) at a given point (r, θ) on outer surface of the tubular cross section with outer radius r is estimated as:

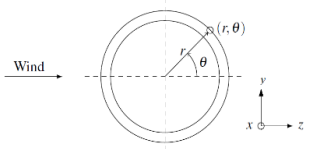

Figure 5 Tubular cross-section local coordinate system

$$\sigma_x = \frac{N_x}{A} - \frac{M_y}{I_y} r \sin(\theta) + \frac{M_z}{I_z} r \cos(\theta) \qquad (2)$$

where A is the cross-sectional area, I_y and I_z are the second moment of area for the cross section computed about the y and z axes, respectively. The shear stress and its resultant fatigue damage has not be taken into account due to its negligible effect relative to the axial stress. The number of load cycles for different stress levels is computed based on rainflow counting technique [34]. The implementation of rainflow cycle counting in WAFO Toolbox [35] has been employed, for bilinear stress versus cycles to failure (S-N) curves [36]. Representative S-N curves were selected based on Det Norske Veritas (DNV) recommended practice [37]. Particularly the curve "D" from Table 2-2 in [37] for steel in seawater with cathodic was selected and since the fatigue damage is pronounced in welds, S-N curves for girth welds were used [36]. A reference thickness equal to 25 mm and a thickness exponent on fatigue strength of 0.2 were used based on [37]. The fatigue damage has been calculated using Palmgren-Miner's rule [37].

4. Results & Discussion

4.1. Sensitivity to operational state

A comparison of the bending moment's power spectral density (PSD) at the mudline for operational and parked state (Figure 6) shows the importance of foundation modelling in the response and consequently in the resultant fatigue damage. For both states, the peak which corresponds to wave excitation has similar energy content for the three models. In the operational state, there is more energy in the range of wave excitation than at the natural frequency, due to the presence of the aerodynamic damping. However, in parked conditions, the resonant response is considerably more important. Additionally, in the operational cases, some response at higher frequencies (over 0.3 Hz) is observed, especially

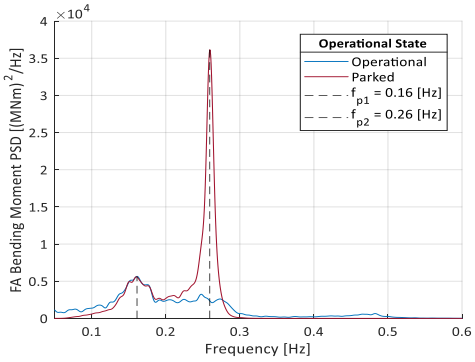

Figure 6 FA bending moment PSD for operational & parked state - M1

around the 3P blade passing frequency. The same behavior can be seen in Figure 7, which shows a comparison of the fore-aft bending moment PSD of model M2 for EC4 for various values of soil damping for the first fore-aft bending mode.

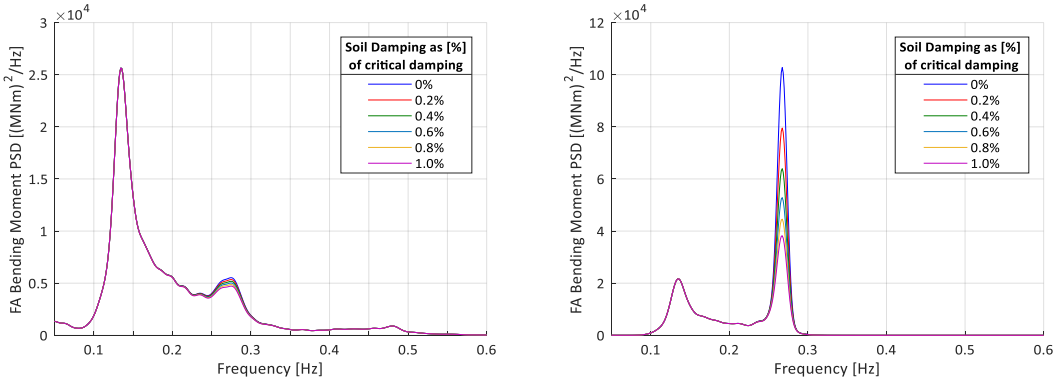

Figure 7 FA Bending Moment PSD for M2 for variations in soil damping ratio in operational (left) and parked (right) state for EC4

Comparing the different soil models, as shown in Figure 8 for both operational and parked states, M2 (linear-elastic foundation stiffness) shows lower amplitudes at the wave frequency excitation, being stiffer than M1 and M3 (non-linear stiffness formulation). In the parked state, the natural frequency for M2 is slightly shifted to the right, while the natural frequency of M3 (with an intermediate stiffness) is observed between M1 and M2. The soil damping effect is clear for the parked cases, where the macro-element predicts lower amplitudes at the natural frequency than M2 and M3.

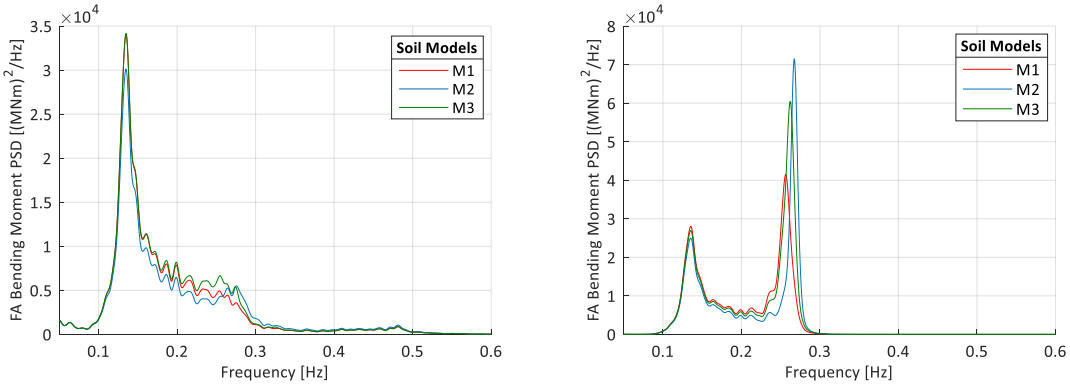

Figure 8 FA bending moment PSD at mudline for operational (left) and parked (right) state [EC4]

In Figure 9, the one-hour fatigue damage at the mudline for M2 and M3 is compared to M1. Positive and negative deviation imply overestimation and underestimation respectively of M2 or M3 compared to M1. In operational states, the variations in fatigue is observed between -10% and 50%. However, the differences in parked states are between -60% to 140% depending on the case. The considerably higher variations in fatigue damage in parked states indicate the increased importance of foundation modelling and inclusion of hysteretic damping effects in cases where aerodynamic damping is negligible.

For operational cases, as shown in Figure 10 (left), the response is dominated by different processes depending on the EC. For EC1, the response close to the 3P frequency range (~ 0.31Hz) dominates due to dynamic amplification, and the differences between foundation models depend on slight differences in the resonant frequency. EC2 is mainly governed by the low frequency component (below 0.05 Hz - Figure 10). This effect resulted in relatively high standard deviation of the axial stress in EC2 (compared to EC3 & EC4), but little fatigue damage, due to the low number of cycles caused by the slowly-varying process. The differences in EC2 are mainly driven by the wave excitation which includes a broad range of frequencies including the natural frequencies, therefore slight variations in the resonant frequency between the soil models may affect the resulting responses. For M2, in EC2-EC3, although the axial

stress standard deviation (STD) was slightly underestimated, the fatigue damage was overestimated compared to M1. Below the resonance frequency, in the region dominated by foundation stiffness, M2 is stiffer than M1, resulting in lower moment amplitudes, while for excitations close to resonance frequency, which are dominated by foundation damping and more important for fatigue, M2 shows higher amplification due to the lower amount of damping. For more severe ECs (4 & 5), waves dominate the response, with high peaks around the wave excitation frequency. In that region, foundation stiffness governs the response, therefore M2's larger stiffness leads to underestimation of the response and damage, while M3 shows a constant overestimation. Also, for the fault case (EC5 – operational) there is a pronounced response close to the natural frequency, likely excited by second order wave loads (from the integration to the instantaneous free surface).

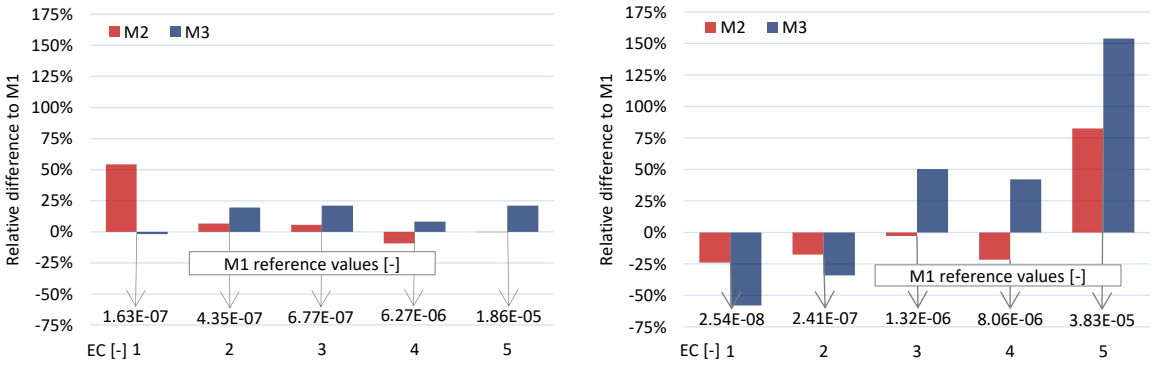

Figure 9 1hr fatigue damage comparisons of M2 and M3 to M1 at mudline for operational (left) and parked (right) state

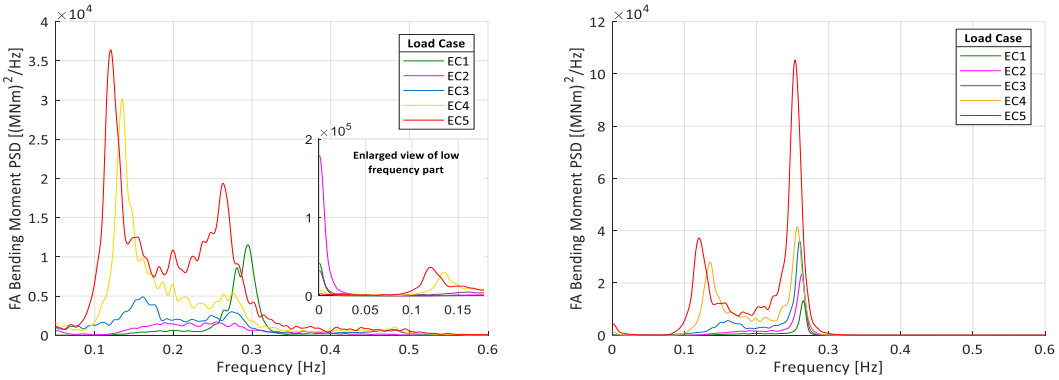

Figure 10 FA Bending Moment PSD of M1 at mudline for different ECs in operational (left) and parked (right) states

In parked cases (Figure 10 - right), the dominant responses for all ECs are close to the natural frequency, where foundation damping dominates. Both M2 and M3 underestimate the responses for EC1 and EC2 and considerably overestimate for EC5. The differences between M2 and M3 rely on the fact that in spite of having the same amount of damping, the different stiffness formulation leads to differences in the resonant frequency, leading to variations in fatigue. The differences of M1 compared to M2 and M3 for high severity ECs is a result of the damping formulation which for M1 increases with higher load amplitudes while for M2 and M3 remains constant (Figure 2). Figure 10 also shows the slight decrease of the resonant frequency due to the foundation stiffness drop for higher load amplitudes.

4.2. Comparison below mudline

Comparing the distribution of the response below seabed between M1 and M3, for both models, the axial stress STD and fatigue damage follow the same behaviour along the monopile giving the maximum values in similar locations. However, as indicated in Figure 11 for EC4, the fatigue damage difference between the two models increases considerably from operational (8.2%) to parked (42.1%) state,

indicating that soil damping contribution has a significant effect in reducing dynamic responses along the monopile, resulting in lower damage over the embedded part of the pile. It should be noted that the difference in estimated maximum fatigue damage below mudline from the different soil models can be larger than the difference of the predicted fatigue damage at the mudline.

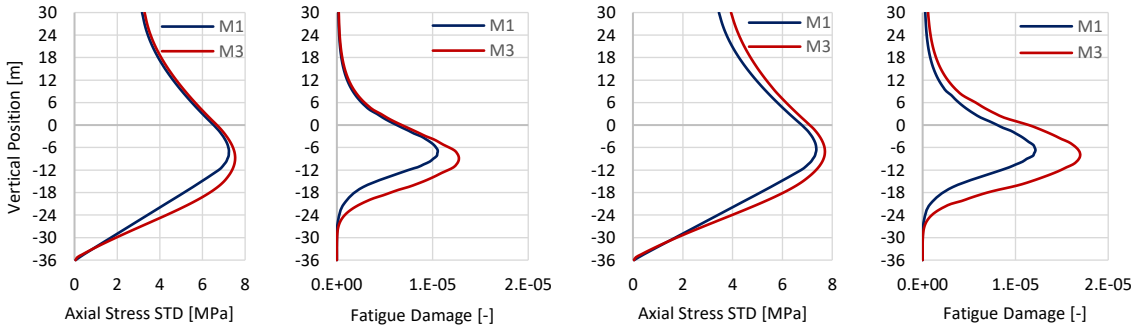

Figure 11 Axial stress STD & fatigue damage along monopile for operational (left) and parked (right) state [EC4]

4.3. Sensitivity to Wind-Wave Misalignment

Considering wind-wave misalignment conditions, Figure 12 shows results at the location (angle) around the monopile with largest fatigue damage – and this location changes for different misalignment angles. In operational cases, EC1 response is dominated by 3P excitations, giving the maximum fatigue damage in the wind direction irrespective of the misalignment angle. Increasing wave misalignment also leads to lower fatigue damage for EC2, and the location of maximum is slightly shifted towards the wave direction for angles higher than 45°. For more severe ECs, dynamic responses due to waves dominate and larger misalignment angles increase maximum fatigue. Different behaviour is observed with respect to the misalignment angle for three frequency ranges. In the *resonance frequency range (0.25 – 0.27 Hz)* for low misalignment angles, aerodynamic damping still capable of attenuating the responses. For angles larger than 45°, aerodynamic damping is negligible in the wave excitation direction, and soil becomes the main contributor of damping. In the *wave frequency range (0.1 – 0.2Hz)* the responses decrease slightly with larger angles of misalignment. In unidirectional wind-waves, the soil experiences higher load levels due to the mean thrust force, resulting in softening of the soil and therefore in slightly higher responses. The responses in the *3P frequency range* decrease with larger misalignment angles, but these responses have minor importance for these ECs. The location of the maximum fatigue damage for ECs 3, 4 and 5 is correlated with the wave direction. The aforementioned effects are shown in Figure 12. In parked cases, fatigue damage constantly decreased with larger misalignment angles mainly due to side-to-side aerodynamic damping as the blades were pitched to 90° in parked conditions. For EC1 and EC2 the fatigue damage was lower than in operational cases for all misalignment angles, while for ECs 3 to 5, the fatigue damage was higher with differences up to 40% for 0°.

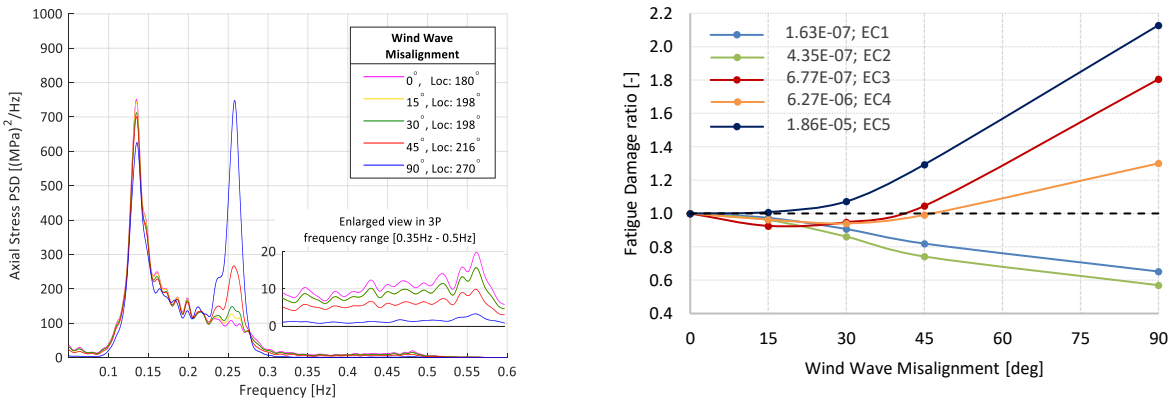

Figure 12 Axial stress PSD at mudline for the point of maximum fatigue damage for EC4 per misalignment angle (left) & maximum fatigue damage ratio per misalignment case to unidirectional operational cases for all ECs (right) for M1

A comparison of the axial stress PSD for the different soil models for high misalignment angles indicates the importance of soil modelling. Figure 13 (left) shows EC4 in operational state with misalignment of 90°. The absence of aerodynamic damping in wave excitation direction, makes soil damping crucial for attenuating the response near natural frequencies, with M1 providing with much lower stress amplitudes. The relative difference of the PSD peaks at resonant frequency between M1 and M3 increased from 23% in EC1-EC2 to around 36% for EC3 and EC4 reaching 60% for EC5, indicating that larger load amplitudes lead to higher hysteretic damping. These effects are reflected in the fatigue damage. In all ECs, for misalignment angles up to 30° the relative difference in fatigue damage is comparable to the unidirectional wind-waves cases (aerodynamic damping is effective) with slight variations up to 5 -10%, depending on the EC. However, for larger misalignment, the differences reach 158% (EC3) and 183% (EC2), indicating the importance of soil modelling in these conditions. For M2, in contrast to M3, slight variations up to 8% in relative difference have been found for the whole range of misalignment angles for EC2, EC3, and EC4. For EC5 similar behaviour is observed as in the case of M3, with a steep rise in the relative deviation after 30° of misalignment from to 10% to 67%.

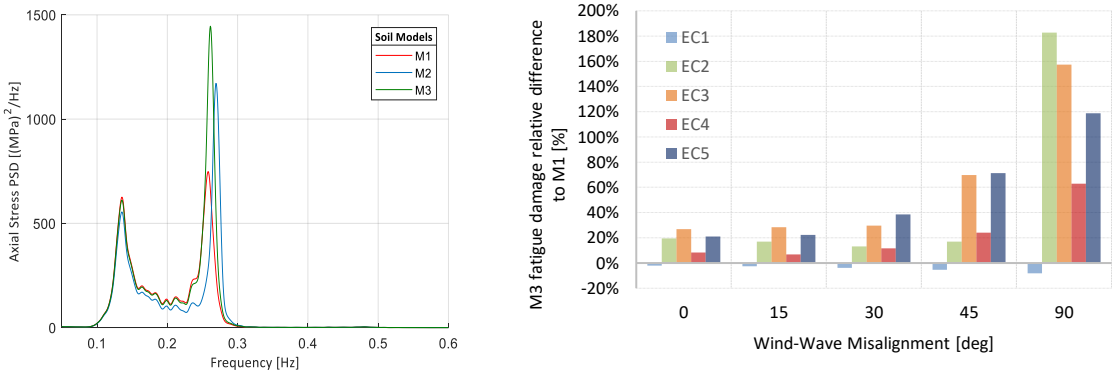

Figure 13 Axial stress PSD for EC4-Operational 90° misalignment (left) Relative difference in fatigue damage at mudline between M1-M3 (right) for different wind-wave misalignment in operational state per EC

Conclusions & Recommendations

Three different models have been used to evaluate short-term fatigue sensitivity in different operational states for the DTU 10MW monopile-based offshore wind turbine; (1) a non-linear elasto-plastic macro element model (M1), (2) a linear elastic model (M2) and (3) a non-linear elastic model (M3). Results show that different processes dominate the responses depending on the environmental state, with both foundation stiffness and damping formulation affecting the behaviour of the models in different frequency regimes. Slight variations in the resonant frequency between the foundation models affected the resulting responses considerably. For all the cases, M2 had lower relative differences than M3 to M1 but this was mainly due to the simplified stiffness formulation which resulted in constant natural frequency for all load levels, in contrast to M1 and M3. In operational states, differences in fatigue damage can vary from -10% to 50%, whereas in parked states differences from -60% to 154% were found, indicating the high importance of foundation modelling and soil hysteretic effects when aerodynamic damping is negligible. Considerable differences have also been found for misalignment angles higher than 30° in operational states, where aerodynamic damping was negligible. Finally, compared to the fatigue damage at mudline, larger variations may occur in the embedded part of the monopile, where the absolute maximum was found for all the cases analysed. To evaluate the long-term effect of the different foundation models on fatigue damage, it is recommended to perform a complete study including long-term probability of occurrence of various sea-states, wind-wave misalignment and OWT operability percentage.

Acknowledgments
The authors gratefully acknowledge the support from the Wave Loads and Soil Support for Extra-Large Monopiles (WASXL) project (NFR grant 268182). The constructive suggestions and comments from Professor Sverre Haver are kindly appreciated.

References

[1] Hundleby G and Freeman K 2017 Unleashing Europe's offshore wind potential - A new resource assessment. WindEurope - BVG Associates)
[2] Remy T and Mbistrova A 2018 Offshore Wind in Europe - Key trends and statistics 2017. WindEurope)
[3] 2015 ORE (Offshore Renewable Energy) Catapult, Cost Reduction Monitoring Framework. In: *Summary Report to the Offshore Wind Programme Board,*
[4] IEC 2009 International Electrotechnical Commission; Design Requirements of offshore wind turbines (IEC 61400-3).
[5] Corbetta G, Pineda I, Moccia J and Guillet J 2014 The European Offshore Wind Industry - Key Trends and Statistics 2013. European Wind Energy Association (EWEA)
[6] Hermans K W P, J.M. 2016 Future XL monopile foundation design for a 10MW wind turbine in deep water. ECN Project)
[7] Schafhirt S, Page A, Eiksund G R and Muskulus M 2016 Influence of Soil Parameters on the Fatigue Lifetime of Offshore Wind Turbines with Monopile Support Structure *Energy Procedia* **94** 347–56
[8] Aasen S, Page A M, Skau K S and Nygaard T A 2017 Effect of foundation modelling on the fatigue lifetime of a monopile-based offshore wind turbine. In: *Wind Energy Science,* pp 361-76
[9] Damgaard M, Zania V, Andersen L V and Ibsen L B 2014 Effects of soil–structure interaction on real time dynamic response of offshore wind turbines on monopiles *Engineering Structures* **75** 388–401
[10] Damgaard M, Andersen L V, Ibsen L B, Tot H S and Sørensen J D 2015 A probabilistic analysis of the dynamic response of monopile foundations: Soil variability and its consequences *Probabilistic Engineering Mechanics* **41** 46–59
[11] Page A, Schafhirt S, Eiksund G, Skau K, Jostad H P and Sturm H 2016 Alternative Numerical Pile Foundation Models for Integrated Analyses of Monopile-based Offshore Wind Turbines. In: *Twenty-sixth International Ocean and Polar Engineering Conference,*
[12] API 2014 API Recommended Practice 2A-WSD; Planning, Designing, and Constructing Fixed Offshore Platforms Working Stress Design; 22 Edition.
[13] Doherty P and Gavin K 2011 Laterally loaded monopile design for offshore wind farms. In: *Proceedings of the Institution of Civil Engineers,*
[14] Page A, Grimstad G, Eiksund G and Jostad H P 2018 A macro-element pile foundation model for integrated analyses of monopile based offshore wind turbines *Ocean Engineering* **167** 23-35
[15] Byrne B W and Houlsby G T 2003 Foundations for offshore wind turbines *Philosophical Transactions of The Royal Society A Mathematical Physical and Engineering Sciences* **361** 2909-30
[16] Page A, Skau K, Jostad H P and Eiksund G 2017 A New Foundation Model for Integrated Analyses of Monopile-based Ofshore Wind Turbines. In: *14th Deep Sea Offshore Wind R&D Conference - EERA DeepWind'17,* (Norway)
[17] Hald T, Mørch C, Jensen L, Bakmar C and Ahle K 2009 Revisiting monopile design using py curves. Results from full scale measurements on Horns Rev. In: *Proceedings of European Offshore Wind 2009 Conference,*

[18] Passon P, Branner K, Larsen S E and Hvenekær Rasmussen J 2015 Offshore Wind Turbine Foundation Design. In: *DTU Wind Energy,*
[19] Smilden E, Bachynski E E and Sørensen A J 2017 Key Contributors to Lifetime Accumulated Fatigue Damage in an Offshore Wind Turbine Support Structure. In: *36th International Conference on Ocean, Offshore and Arctic Engineering (OMAE),*
[20] Bienen B, Byrne B W, Houlsby G T and Cassidy M J 2006 Investigating six-degree-of-freedom loading of shallow foundations on sand *Géotechnique* **56** 367-79
[21] Correia A 2011 A Pile-head Macro-element Approach to Seismic Design of monoshaft supported bridges. (Pavia, Italy: European School for Advanced Studies in Reduction of Seismic Risk, ROSE School)
[22] Houlsby G T and Cassidy M J 2002 A plasticity model for the behaviour of footings on sand under combined loading *Géotechnique* **52** 117-29
[23] Skau K S, Grimstad G, Page A M, Eiksund G R and Jostad H P 2017 A macro-element for integrated time domain analyses representing bucket foundations for offshore wind turbines *Marine Structures,* **59** 158-78
[24] Tistel J, Grimstad G and Eiksund G R 2017 A macro model for shallow foundations on granular soils describing non-linear foundation behavior *Computers & Structures*
[25] Iwan W D 1967 On a Class of Models for the Yielding Behavior of Continuous and Composite Systems *Journal of Applied Mechanics* **34**
[26] Page A, Grimstad G, Eiksund G and Jostad H P 2019 A macro-element model for multidirectional cyclic lateral loading of monopiles in clay *Computers and Geotechnics* **106** 314–26
[27] Bak C, Zahle F, Bitsche R, Kim T, Yde A, Henriksen L C, Natarajan A and Hansen M 2013 Description of the DTU 10 MW Reference Wind Turbine. Technical University of Denmark)
[28] Jonkman B J 2009 TurbSim user's guide: Version 1.50, Technical Report. National Renewable Energy Lab (NREL)
[29] Lin L, Zhen G and Torgeir M 2013 Joint Environmental Data at Five European Offshore Sites for Design of Combined Wind and Wave Energy Devices. In: *International Conference on Ocean, Offshore and Arctic Engineering (OMAE),*
[30] Page A M, Næss V, De Vaal J B, Eiksund G R and Nygaard T A 2019 Impact of foundation modelling in offshore wind turbines: Comparison between simulations and field data. *Marine Structures* **64** 379-400
[31] Tarp-Johansen N J, Mørch C, Andersen L, Christensen E D and Frandsen S T 2009 Comparing Sources of Damping of Cross-Wind Motion. In: *European Offshore Wind 2009: Conference & Exhibition - The European Wind Energy Association,*
[32] Damgaard M, Andersen J, Ibsen L B and Andersen L 2012 Time-varying dynamic properties of offshore wind turbines evaluated by modal testing. In: *Proceedings of the 18th international conference on soil mechanics and geotechnical engineering,* pp 2343-6
[33] WindEnergie G L G 2005 Overall damping for piled offshore support structures, guideline for the certification of offshore wind turbines.
[34] Matsuishi M and Endo T 1968 Fatigue of metals subjected to varying stress. In: *Kyushu Branch of Jpan Society of Mechanics Engineering,* pp 37-40
[35] Brodtkorb P, Johannesson P, Lindgren G, Rychlik I, Ryden J and Sjo E 2000 WAFO—A MATLAB Toolbox for the Analysis of Random Waves and Loads. In: *10th International Offshore and Polar Engineering Conference (ISOPE),* pp 343–50
[36] Bachynski E E, Kvittem M I, Luan C and Moan T 2014 Wind-Wave Misalignment Effects on Floating Wind Turbines: Motions and Tower Load Effects *Journal of Offshore Mechanics and Arctic Engineering* **136**
[37] DNVGL (Det Norske Veritas-Germanischer Lloyd), 2016 Fatigue design of offshore steel structures.